Vibrational molecular modulation in hydrogen

Shu Wei Huang,[1,*] Wei-Jan Chen,[1] and A. H. Kung[1,2,†]
[1]*Institute of Atomic and Molecular Sciences, Academia Sinica, Taiwan, Republic of China*
[2]*Department of Photonics, National Chiao-Tung University, Hsinchu, Taiwan, Republic of China*
(Received 15 July 2006; published 26 December 2006)

Detailed numerical modeling of using the vibrational coherence of H_2 for molecular modulation is presented. The focus of the calculation is on a strongly driven system aimed at producing many sidebands in the presence of Doppler broadening and the effects of collisions at room temperature. It is shown that Dicke narrowing that reduces the Doppler width plays a critical role in high order sideband generation in room temperature H_2. In addition, the calculation shows that generation of many sidebands favors the phased state as has been reported in all gas phase experiments and is primarily a consequence of the Stark shifts that result from the applied high intensities. The influence of self-focusing in the gas medium that has been conjectured in previous studies is only secondary. The numerical results agree with experimental data obtained in our laboratory, where we have succeeded in generating collinearly propagating Raman sidebands with wavelengths that range from 2216 nm in the infrared to 133 nm in the vacuum ultraviolet. The frequencies covered by these sidebands span over four octaves for a total of more than 70 600 cm^{-1} in the optical region of the spectrum.

DOI: 10.1103/PhysRevA.74.063825 PACS number(s): 42.50.Gy, 42.65.Dr, 33.80.−b, 42.65.Re

I. INTRODUCTION

The rise in interest in attosecond science has stimulated intense efforts in the past decade to generate subfemtosecond and attosecond pulses. Due to the uncertainty principle, a prerequisite to subfemtosecond pulse duration is for the light pulse to have a sufficiently broad electromagnetic spectral width so that equivalently through Fourier transformation the pulse is short in time. Two techniques, high-order harmonic generation [1–6] and high-order collinear Raman sideband generation [7–19], have surfaced as the most promising techniques to produce pulses with a phase coherent spectrum broad enough for compression to less than one femtosecond in duration. Pulses shorter than 200 attoseconds were demonstrated using high-order harmonic generation [6]. While this approach has produced the shortest pulse duration, the peak power is low, owing to the typical 10^{-7}–10^{-9} conversion of the high harmonic generation process, and the generated photon energy falls in the 30–100 eV range. It is therefore not possible to use these pulses to study electron dynamics in the lower energy region. In contrast, high-order collinear Raman sideband generation produces pulses in the optical region from the infrared to the deep-uv and the process has been shown to have near-unity conversion efficiency in producing a broad spectrum [15].

It is now understood, due to detailed work of the Harris group and supplemented by the Hakuta group, that when a molecular Raman transition is driven adiabatically by two high intensity lasers so that the molecular coherence approaches its maximum value of 0.5, the laser pulse frequencies will be modulated to produce many sidebands that propagate collinearly with the driving laser beams. The modulation frequency (frequency spacing between adjacent sidebands) is equal to the difference of the frequencies of the two driving lasers. Efficient molecular modulation has since been demonstrated in gaseous D_2, rotationally excited para-H_2, and in vibrating solid and liquid H_2, generating sidebands that span up to ~50 000 cm^{-1} in spectral coverage [12–14,16]. Pulses generated in D_2 have been compressed to produce a train of near-single-cycle pulses with a pulse envelop width of 1.6 fs and a peak power as high as 1 MW [18]. More recently, an in-depth experimental study on molecular modulation in D_2 that confirms much of the observations of the earlier studies was reported [17].

Gas phase H_2 is well known to be a very efficient vibrational Raman scattering medium. The $Q(1)$ [$v=0$, $J=1\rightarrow v=1$, $J=1$] vibrational Raman transition of H_2 is one of the strongest Raman transitions of all molecules. Having a transition frequency of 4155.2 cm^{-1}, largest among all molecules, means it will require the fewest number of sidebands for H_2 [$Q(1)$] to cover the same modulated bandwidth. At room temperature, nearly 67% of the ground state molecules reside in the $J=1$ state. Hence, unlike the D_2 and rotational para-H_2 experiments that were all conducted at cryogenic temperature, H_2 could be operated at room temperature and still produce strong modulation by one dominant transition. In addition, H_2 possesses the most complete and reliable set of spectroscopic and dynamical data, such as its energy level positions [20], dipole matrix elements [21], absorption cross sections, and Doppler and collisional broadening coefficients [22,23], to allow accurate modeling of the molecular modulation process. These factors therefore make vibrational H_2 an excellent candidate for producing a wide spectrum of sidebands by molecular modulation for the purpose of subfemtosecond generation. On the other hand, H_2 being the lightest molecule has a large Doppler width of 1.1 GHz at 300 K. This has a significant negative effect on the efficiency of the modulation process since the driven coherence will be reduced in value as a result of Doppler averaging when the laser excitation is tuned onto or near the Raman resonance [13,24].

*Present address: Department of Electrical Engineering and Computer Science, M.I.T., Cambridge, MA.
†Email address: akung@pub.iams.sinica.edu.tw

We have performed detailed numerical modeling of using the vibrational coherence of H_2 for molecular modulation. The focus of the calculation is on a strongly driven system aimed at producing many sidebands in the presence of room temperature Doppler broadening and the effects of collisions. In this paper, we report the details of our numerical calculation including comparison with the result of experiments done in our laboratory. We show that Dicke narrowing that reduces the Doppler width [25,26] plays a critical role in sideband generation in H_2. In addition, generation of high order sidebands favoring the phased state that has been reported in gas phase experiments [13,17] is primarily a consequence of the Stark shifts under the high applied laser intensities. The influence of self-focusing in the gas as was conjectured in previous studies [13,17] is only secondary. Experimentally, we have succeeded in generating collinearly propagating Raman sidebands with wavelengths that range from 2216 nm in the infrared to 133 nm in the vacuum ultraviolet. The frequency range covered by these sidebands spans over four octaves for a total of more than 70 600 cm^{-1} in the optical region of the spectrum. In Sec. II of this paper we review the essential theory that is pertinent to our study. Section III gives the details of our numerical approach. In Sec. IV we present the result of the calculations. Section V is a comparison with experimental results in room temperature H_2 followed by a conclusion in Sec. VI.

II. THEORETICAL FORMULATION

The basic formalism for establishing a strong coherence by applying two intense slightly off-resonance laser fields was first described by Harris and Sokolov [8] and later analyzed in detail by Le Kien *et al.* [19]. We rely on the analyses by these two groups to formulate our modeling of the H_2 system. For the sake of completeness, the formulation and essential conclusions from these references are reproduced here since they serve as the basis in the development of the rest of this paper.

The interaction of two driving lasers with a molecular medium can be described by the multilevel system depicted in Fig. 1. The transition between vibrational states a and b is electric dipole forbidden and the frequencies of the two driving lasers are such that $\omega_0-\omega_{-1}=\omega_b-\omega_a-\delta$, where $\omega_b-\omega_a$ is the energy difference of states a and b and δ is the two-photon detuning. The frequencies ω_0 and ω_{-1} are far off resonance from the transitions between states j and either a or b so the one-photon detuning is large compared to the Rabi frequency Ω_{ab} and the two-photon detuning. Under these assumptions the problem can be simplified to that of a two-level system with an effective Hamiltonian [8,19]:

$$H_{\text{eff}} = -\hbar \begin{bmatrix} \Omega_{aa} & \Omega_{ab} \\ \Omega_{ba} & \Omega_{bb} - \delta \end{bmatrix}. \tag{1}$$

The Starks shifts Ω_{aa} and Ω_{bb} and the complex two-photon Rabi frequencies Ω_{ab} and Ω_{ba} are given by

$$\Omega_{aa} = \frac{1}{2}\sum_q a_q |E_q|^2,$$

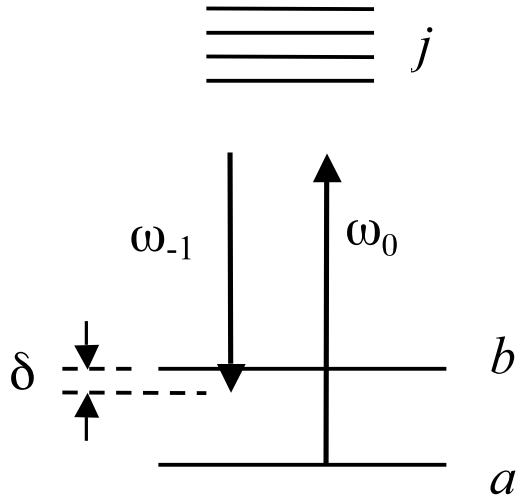

FIG. 1. Energy level diagram. Levels a and b are coupled with levels j by $E(\omega_0)$ and $E(\omega_{-1})$. The transition between levels a and b is electric dipole forbidden. $\omega_0-\omega_{-1}$ is tuned off from two-photon resonance by a detuning δ. ω_0 and ω_{-1} are far off resonance from the one-photon transition between states j and either a or b.

$$\Omega_{bb} = \frac{1}{2}\sum_q b_q |E_q|^2,$$

$$\Omega_{ab} = \Omega_{ba}^* = \frac{1}{2}\sum_q d_q E_q E_{q+1}^*, \tag{2}$$

where E_q stands for the complex field envelope of the qth Raman sideband.

The constants a_q, b_q, d_q in Eqs. (2) which determine the dispersion and the coupling are given by

$$a_q = \frac{1}{2\hbar^2}\sum_j \left(\frac{|\mu_{ja}|^2}{\omega_j - \omega_a - \omega_q} + \frac{|\mu_{ja}|^2}{\omega_j - \omega_a + \omega_q} \right),$$

$$b_q = \frac{1}{2\hbar^2}\sum_j \left(\frac{|\mu_{jb}|^2}{\omega_j - \omega_b - \omega_q} + \frac{|\mu_{jb}|^2}{\omega_j - \omega_b + \omega_q} \right),$$

$$d_q = \frac{1}{2\hbar^2}\sum_j \left(\frac{\mu_{aj}\mu_{jb}}{\omega_j - \omega_b - \omega_q} + \frac{\mu_{aj}\mu_{jb}}{\omega_j - \omega_a + \omega_q} \right), \tag{3}$$

where μ_{ja} and μ_{jb} are the dipole moments of the transitions $j \leftrightarrow a$ and $j \leftrightarrow b$, respectively. $\omega_q = \omega_0 + q(\omega_b - \omega_a - \delta)$ is the frequency of the qth Raman sideband.

The eigenvalues $E_{\text{eff}}^{\pm} = -\hbar\lambda^{(\pm)}$ of the Hamiltonian in Eq. (1) have been shown [13,19] to be

$$\lambda^{(\pm)} = \frac{1}{2}(\Omega_{aa} + \Omega_{bb} - \delta) \pm \frac{1}{2}\sqrt{(\Omega_{aa} - \Omega_{bb} + \delta)^2 + 4|\Omega_{ab}|^2} \tag{4}$$

with the associated eigenvectors being

$$|\pm\rangle = \cos\theta^{(\pm)}|a\rangle + \sin\theta^{(\pm)} e^{-i\varphi}|b\rangle, \tag{5}$$

where φ is such that $\Omega_{ab} = |\Omega_{ab}| e^{i\varphi}$ and

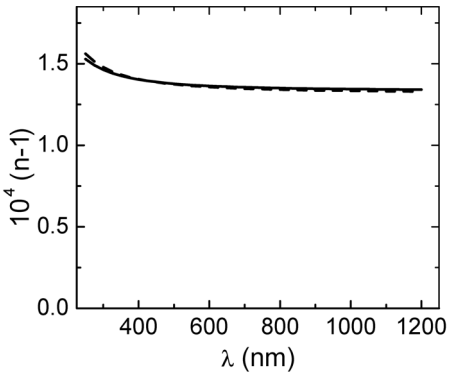

FIG. 2. The refractive index n in the form $n-1$ as a function of wavelength. The solid line is calculated from Eq. 12 of Ref. [28] while the dashed line is calculated using Eq. (11) with rescaled dipole moments (see text).

$$\tan\theta^{(\pm)} = \frac{2|\Omega_{ab}|}{\Omega_{aa} - \Omega_{bb} + \delta \pm \sqrt{(\Omega_{aa} - \Omega_{bb} + \delta)^2 + 4|\Omega_{ab}|^2}}. \tag{6}$$

The coherence ρ_{ab} of the superposition of states a and b induced by the laser fields can be expressed in terms of θ as

$$\rho_{ab}^{(\pm)} = \frac{1}{2}e^{i\varphi}\sin 2\theta^{(\pm)} = \pm \frac{\Omega_{ab}}{\sqrt{(\Omega_{aa} - \Omega_{bb} + \delta)^2 + 4|\Omega_{ab}|^2}} \tag{7}$$

which shows that max $|\rho_{ab}|=0.5$, arrived at when

$$|\Omega_{ab}| \gg |\Omega_{aa} - \Omega_{bb} + \delta|. \tag{8}$$

In other words, maximum coherence can be achieved only when the magnitude of the Rabi frequency Ω_{ab} is sufficiently larger than the absolute sum of the off-resonance detuning δ and the net Stark shift Ω_{aa}-Ω_{bb} [19].

The density-matrix equations that govern the evolution of the states in the presence of decay in the medium in local coordinates then are

$$\frac{\partial\rho_{aa}}{\partial\tau} = i(\Omega_{ab}\rho_{ba} - \Omega_{ba}\rho_{ab}) + \gamma_{\parallel}\rho_{bb},$$

$$\frac{\partial\rho_{bb}}{\partial\tau} = -i(\Omega_{ab}\rho_{ba} - \Omega_{ba}\rho_{ab}) - \gamma_b\rho_{bb},$$

$$\frac{\partial\rho_{ab}}{\partial\tau} = i(\Omega_{aa} - \Omega_{bb} + \delta + i\gamma_{\perp})\rho_{ab} + i\Omega_{ab}(\rho_{bb} - \rho_{aa}), \tag{9}$$

where ρ_{aa} and ρ_{bb} are the level population of state a and state b, respectively, $\gamma_{\parallel}$ stands for the decay rate from state b to a, γ_b is the total decay rate from b that gives the Raman transition linewidth, and $\gamma_{\perp}$ is the dephasing rate of the coherence ρ_{ab}. Equations (2), (3), and (9) can be solved for the level population ρ_{aa} and ρ_{bb} and the coherence ρ_{ab}, which are elements of a 2×2 density matrix of the two level system in the presence of the driving laser fields and the sidebands. Under the slowly varying envelope approximation, propagation of the qth sideband in local time is written as [8,19]

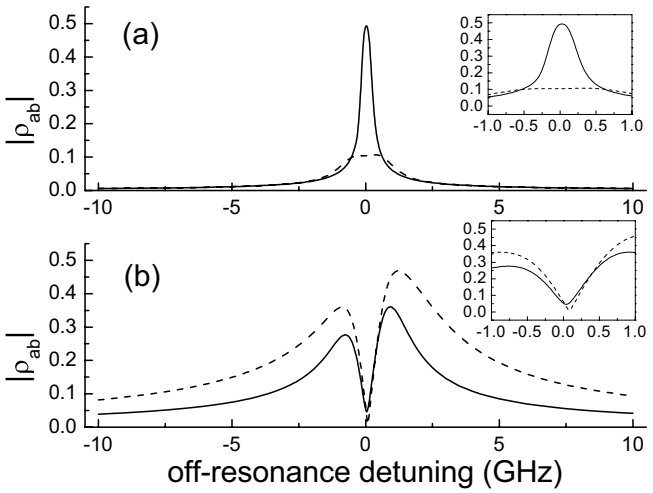

FIG. 3. Calculated initial Raman coherence $|\rho_{ab}|^{(0)}$ as a function of off-resonance detuning at 10 Torr at various driving laser intensities. (a) $I(\omega_0)=I(\omega_{-1})=1$ GW/cm^2. The solid line in (a) is the ideal case with no Doppler effect while the dashed line represents the result including the Doppler effect. (b) The driving laser intensities are $I(\omega_0)=I(\omega_{-1})=7$ GW/cm^2 for the solid line while those for the dashed line are $I(\omega_0)=12$ GW/cm^2 and $I(\omega_{-1})=20$ GW/cm^2. The Doppler effect is included in the two cases in (b). The horizontal scales in (a) and (b) are expanded in the insets to display a small intensity-dependent shift of the minimum of the dip in the coherence from the Raman resonance.

$$\frac{\partial E_q}{\partial z} = -j\eta\omega_q N[(a_q\rho_{aa}E_q + b_q\rho_{bb}E_q) + (d_{q-1}\rho_{ba}E_{q-1} + d_q^*\rho_{ab}E_{q+1})], \tag{10}$$

where N is the molecular gas density and η is the characteristic impedance. The two terms inside the first round brackets on the right-hand side of Eq. (10) give the dispersion of the system, and the two terms inside the second round brackets couple E_q to the adjacent sidebands. The solution of this equation gives the field amplitude of all the sidebands that result from the interaction of the driving lasers with the medium. When the magnitude of the coherence ρ_{ab} is near its maximum value of 0.5, the coupling terms in Eq. (10) are of the same order of magnitude as the dispersion terms. Efficient conversion of the incident fields to the new sidebands occurs within one coherence length so that phase matching is not necessary. Consequently the incident fields and all the fields generated within this regime propagate collinearly through the coherent medium.

Equations (9) and (10) form the basis of our modeling of the H_2 vibrational system. Since H_2 has many upper vibronic states each coupled to the states a and b with a different Franck-Condon factor and since it is important to include the molecular decay rates and the Doppler effect in the model, it is necessary to use numerical techniques to solve this set of equations to obtain the final results.

III. NUMERICAL SIMULATION

Our calculation is for H_2 at a temperature of 300 K. We shall consider only the frequency range that is far off reso-

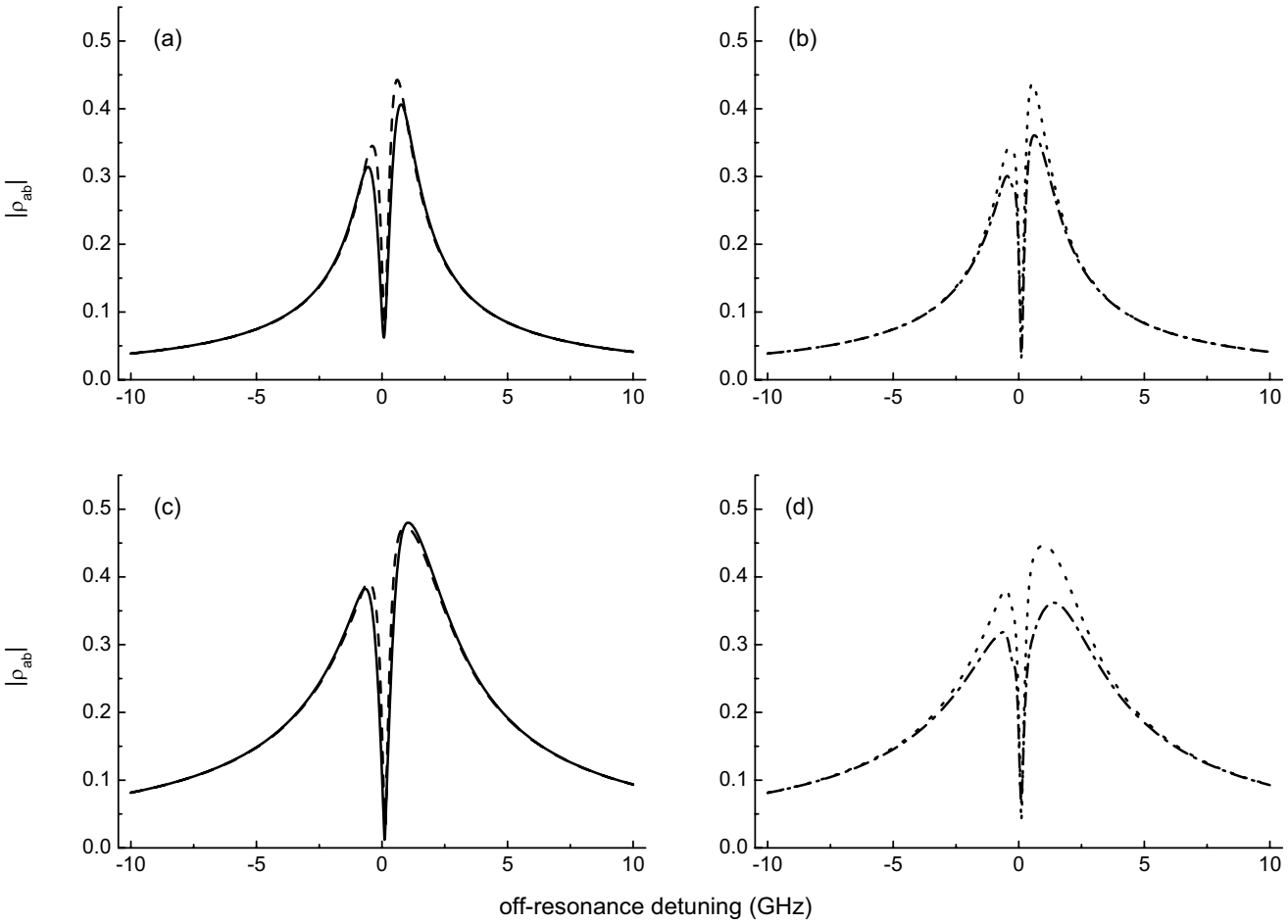

FIG. 4. Calculated initial Raman coherence as a function of off-resonance detuning at various pressures with driving laser intensities: (a) and (b) $I(\omega_0)=I(\omega_{-1})=7$ GW/cm^2; (c) and (d) $I(\omega_0)=12$ GW/cm^2 and $I(\omega_{-1})=20$ GW/cm^2. The H_2 pressure is 200 Torr for the solid line, 500 Torr for the dashed line, 1000 Torr for the dotted line, and 3000 Torr for the dashed dotted line.

nance from the upper electronic states and for $\omega_0-\omega_{-1}$ close to the $Q(1)$ Raman resonance. The dispersion constants a_q and b_q and the coupling constants d_q include the contributions of the 0–36th vibrational transitions of the Lyman band and 0–13th transitions of the Werner band. As for the transition dipole moments we use the set calculated and provided to us by Le Kien [19,27]. This set includes both the magnitudes and the relative signs of the dipole matrix elements. Recognizing that the linear dispersion for H_2 calculated using the well-developed expression

$$n_q - 1 = \frac{N\hbar a_q}{\varepsilon_0}, \tag{11}$$

with these matrix elements does not reconcile with the published linear H_2 dispersion [27], we first attempted to include another term in Eq. (11) to represent all other high energy electronic states to the system but this still failed to match the linear dispersion and satisfy the oscillator strength sum rule simultaneously. We then found empirically that by scaling the $(\mu_{ij})^2$ by a factor of $\sqrt{3}$ the linear dispersion calculated then agrees quite well with those derived from the sum rules and the reported measurements [28] (Fig. 2). Since this scaling factor gives a good fit to the dispersion data over a broad spectral range, we feel it is justified to include the factor throughout our simulation.

Parameters of the driving lasers are taken from the lasers used in the H_2 experiments in our laboratory. The lasers have Gaussian temporal profiles with duration of 5 ns and

TABLE I. Doppler widths for several hydrogen pressures at 300 K [22].

Pressure (Torr)	Doppler width (MHz)
10	1100
200	775
500	480
700	403
1000	313.3
1500	260
2000	248.8
3000	268
5000	357.5

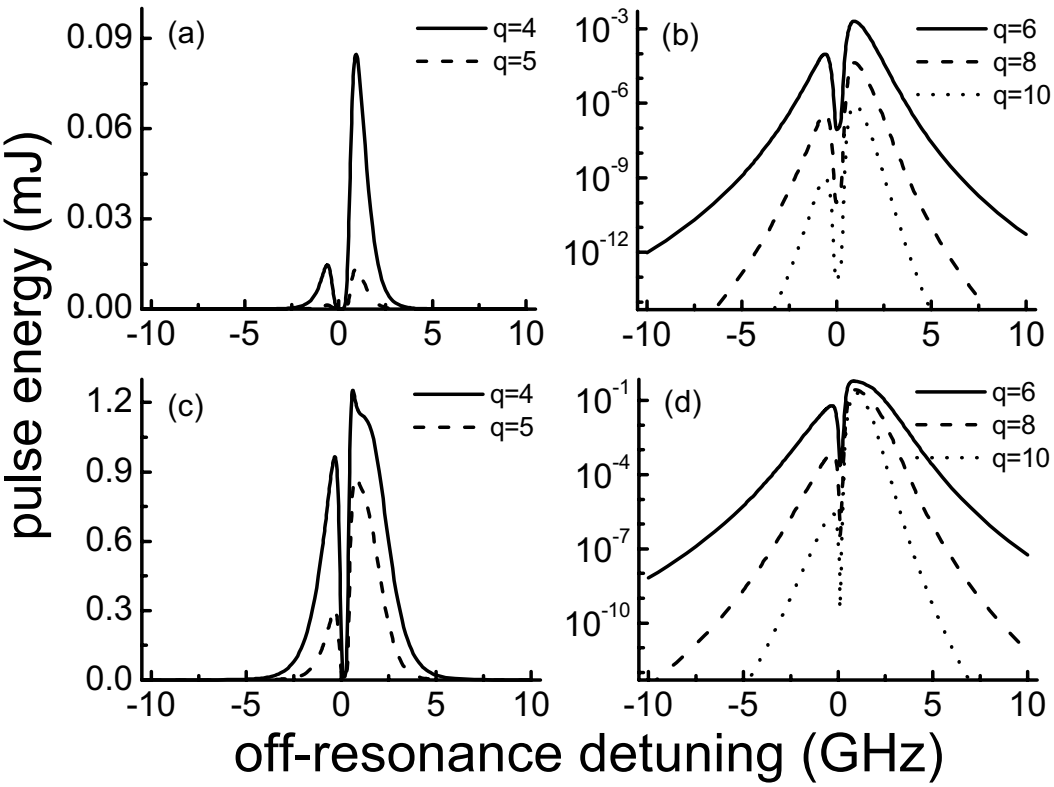

FIG. 5. Calculated generated sideband energies as a function of off-resonance detuning in (a), (b) 200 Torr and (c), (d) 500 Torr H_2 with driving laser intensities of $I(\omega_0)=12$ GW/cm^2 and $I(\omega_{-1})=20$ GW/cm^2. q is the order of the anti-Stokes sideband.

bandwidths of ~100 MHz. The laser frequencies are $\omega_0=16\,978.2$ cm^{-1} (dye) and $\omega_{-1}=12\,823$ cm^{-1} (Ti:sapphire). The frequency of the $Q(1)$ Raman transition is 4155.2 cm^{-1} and we change the off-resonance detuning δ by varying ω_{-1}. Since the Raman linewidth of $Q(1)$ is small [22], the decay rate γ_b is set equal to the laser bandwidth and the internal decay rate $\gamma_\parallel$ is neglected. The dephasing rate $\gamma_\perp$ of 51.3 MHz/amagat is taken from [22]. The amplitude of the applied fields at $z=0$ are $E_0(0)$ and $E_{-1}(0)$ given by the incident intensities $I_i(0)=[E_i(0)]^2/2\eta$, where η is $\sqrt{(\mu_o/\varepsilon_o)}\approx 377$ and $i=0,-1$. In the simulation E_{-1} is incident into the cell ahead of E_0 by 1 ns. Evolution of the sidebands $E_{-4}(z)$ to $E_{15}(z)$ is followed throughout the calculation. We assume a top-hat spatial profile for all the fields and we use the plane wave approximation and neglect the effects of diffraction in the propagation of the fields in the z direction. The focal distance of the driving lasers is 3 cm and this distance is used as the interaction length.

At 300 K 66.6% of the H_2 population resides in the $v=0$, $J=1$ state such that the $Q(1)$ Raman transition dominates. Since we are concerned with a process that is far off resonance from the upper electronic states and we consider only frequency detunings that are close to the $Q(1)$ Raman resonance, we can assume that all molecules contribute to the linear dispersion but only those molecules in the $v=0$, $J=1$ state contribute to the sideband generation. Equation (10) is then modified to become

$$\frac{\partial E_q}{\partial z} = -j\eta\omega_q[N(a_q\rho_{aa}E_q + b_q\rho_{bb}E_q) + \underline{0.666}N(d_{q-1}\rho_{ba}E_{q-1} + d_q^*\rho_{ab}E_{q+1})], \quad (12)$$

where we have underlined the modification factor to the population for the coupling term. We solve this propagation equation and the density-matrix equations numerically in Fortran. For each time segment and at every step along the propagation direction we solve the density-matrix equations to obtain the dispersion and coupling constants by the 4th order Runge-Kutta method proposed by Gill [29]. In this calculation we take into account the Doppler width of H_2 at 300 K that is of the order of 1.0 GHz. This value is in the same ballpark as the Rabi frequencies and is much larger than the laser linewidth. The influence of the Doppler width on the molecular coherence near resonance is significant [13]. The coupling constants as a function of detuning are Doppler averaged to account for the Doppler shift of the laser frequency relative to the Raman resonance at different molecular velocities. We then solve the propagation equation for E_q by the Euler-trapezoidal method with error control, also known as the predictor-corrector method. Integrating over the temporal and spatial profiles gives the final pulse energy of each sideband as a function of the Raman detuning. Note that while the Euler-trapezoidal method with error control provides better convergence, Gill's method provides better efficiency [30]. Hence, by properly applying the two

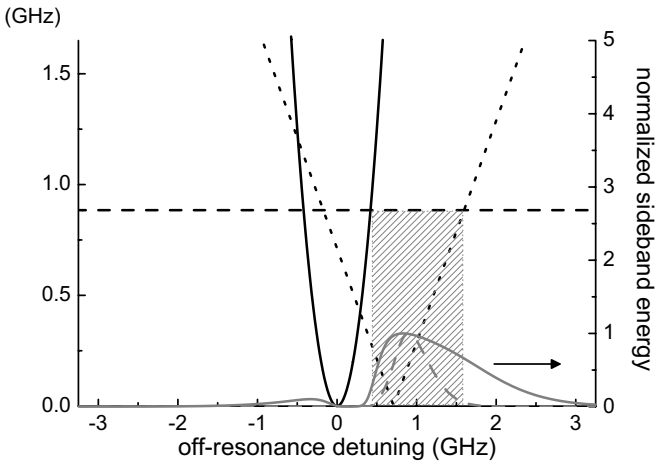

FIG. 6. Plot to indicate the region of detuning that satisfies the conditions for adiabatic following and large coherence. The solid line is $T|\delta|^2$, where T is the FWHM of the driving laser pulses, the dashed line is the magnitude of Rabi frequency $|\Omega_{ab}|$, and the dotted line is $|\Omega_{aa}-\Omega_{bb}+\delta|$, the absolute sum of the detuning and the net Stark shift. The shaded area is the region that meets the requirements for adiabatic following and large coherence. The solid gray line is the normalized energy of the 6th sideband and the dashed gray line is that of the 12th sideband against the detuning which illustrates that the high order sideband generation obeys both conditions.

methods, we can get results of sufficient accuracy without sacrificing calculation speed.

IV. RESULTS AND DISCUSSION

Of utmost concern in using room temperature H_2 is the influence of the large Doppler width in achieving maximum coherence. When the laser excitation is tuned close to the Raman resonance, the adiabatic preparation in both wings of the velocity distribution of the Doppler profile are equal in magnitude but opposite in phase so that the contribution from these molecules to the coherence excitation cancels each other, resulting in a reduced value [13,24]. Figures 3 and 4 show the magnitude of the calculated coherence $|\rho_{ab}|$ at the entrance to the H_2 medium ($|\rho_{ab}|^{(0)}$) as a function of the off-resonance detuning δ at different pressures and driving laser intensities. The damaging effect of a large Doppler width can be clearly seen in Fig. 3. In the absence of the Doppler effect, the coherence can reach its maximum value of 0.5 at a modest laser intensity of 1 GW/cm^2. However, the Doppler averaged coherence drops substantially to about 0.1, a fivefold reduction from its maximum value, at low H_2 pressure where the Doppler linewidth is about 1.1 GHz [Fig. 3(a)]. Even at high intensities, the coherence still could not rise to its theoretical maximum [Fig. 3(b)]. This shows that increasing intensity alone is not sufficient to overcome the damage done to the coherence by the severe Doppler broadening. Incidentally the dip in Fig. 3(b) is a result of Rabi flopping brought on by nonadiabatic population transfer from state a to state b when the detuning is nearly on resonance with the Raman transition. Due to an unequal Stark shift of levels a and b, the bottom of this dip has a slight shift from

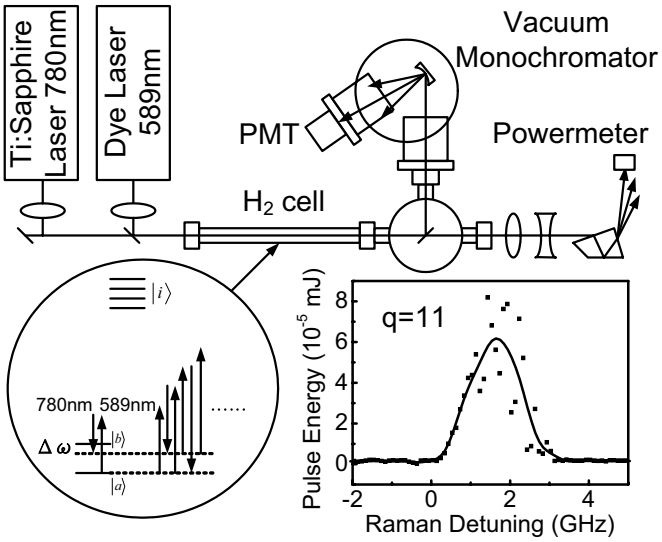

FIG. 7. Schematic of the experimental setup. The inset shows the measured sideband energy of the 11th anti-Stokes output at 160 nm in 500 Torr H_2. Square dots are the experimental data points. The solid line is a polynomial fit of the data.

the low intensity Raman resonance (zero detuning). This shift is most obvious at high intensities as shown in the inset in Fig. 3.

At higher pressures, the Doppler width is reduced by Dicke narrowing [25,26]. Table I shows the linewidth of the $Q(1)$ Raman transition of H_2 extracted from Fig. 3 and Eq. (1) in [22]. The table shows that the linewidth changes from ~1.1 GHz at low pressure to ~250 MHz at 2000 Torr before increasing again as a consequence of collisional broadening [22,23]. Figure 4 shows the calculated initial coherence at H_2 pressures of 200 to 3000 Torr. Compared with Fig. 3 we see that the reduction in the Raman linewidth at intermediate pressures has enhanced the magnitude of the coherence. At 7 GW/cm^2, the magnitude of the coherence at $z=0$, $|\rho_{ab}|^{(0)}$, reaches 0.45 at 500 Torr but starts to drop at 1000 Torr. If we increase the driving laser intensity to 12 GW/cm^2 for ω_0 and 20 GW/cm^2 for ω_{-1} (to match what we have in our experiment), which also increases the Stark shift, the coherence can reach close to the maximum value of 0.5 at 200 and 500 Torr with positive off-resonance detuning [Fig. 4(c)]. Figure 4 also shows that the influence of collision-induced dephasing on the coherence begins to be felt above 700–1000 Torr for the 5 ns pulse duration.

Solving for the coherence and Eq. (12) as the laser pulses propagate through the medium gives the generated pulse energy of each sideband in the collinear direction. Figures 5(a) and 5(b) display the calculated single pulse energy of the sidebands generated in 200 and 500 Torr H_2 under the conditions of Fig. 4(b). We notice that, first, many orders of Raman sidebands can be generated. Second, high-order sidebands are generated only when the coherence is near its maximal value of 0.5. As has been emphasized by Harris and Sokolov [13] and discussed in Sec. II, efficient sideband generation occurs when $|\rho_{ab}|^{(0)}$ is near its maximum of 0.5 such that the coupling term is comparable to the dispersion term in the propagation equation. Room temperature H_2 is more

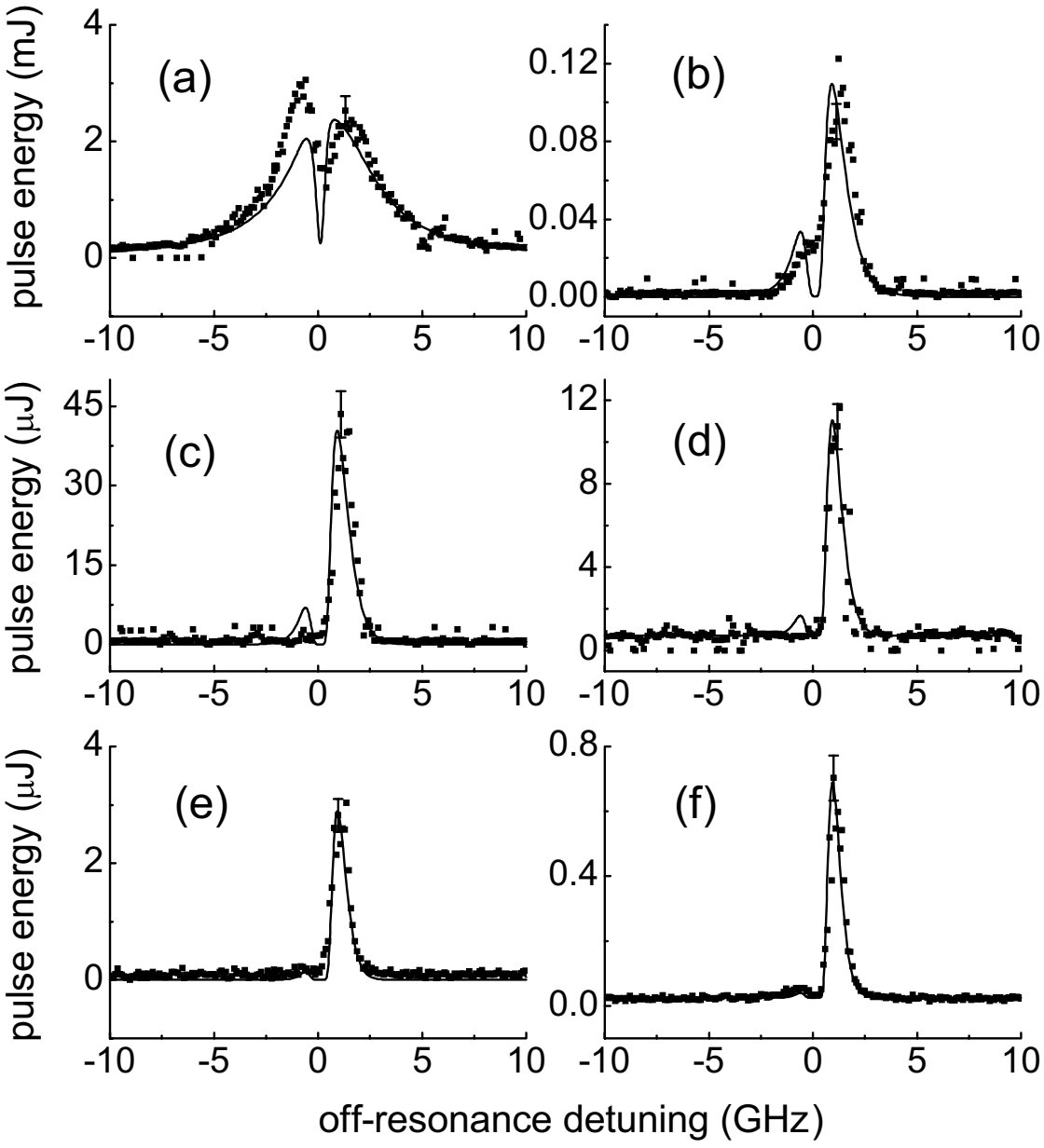

FIG. 8. Measured energy of representative anti-Stokes radiation generated in 200 Torr H_2 for sideband orders: (a) $q=1$, (b) $q=3$, (c) $q=4$, (d) $q=5$, (e) $q=6$, and (f) $q=7$. The square dots are the experimental data points. The solid lines are values calculated under the experimental conditions used and matched to the highest measured output at positive detuning. There are no other free parameters. The error bar indicates the typical one standard deviation fluctuation of the signal near its peak value.

sensitive to this condition due to the dilution in its population in the $v=0$, $J=1$ state. From Figs. 4 and 5, we see that only when the detuning is near +1 GHz where $|\rho_{ab}|^{(0)}$ is well above 0.4 that high-order sidebands are generated with a reasonable efficiency. Moreover, the calculation shows that high-order generation favors positive detuning when the driven molecular coherence is in phase with the driving laser fields and is not nearly as effective for negative detuning when the coherence and the driving laser fields are 180° out of phase (antiphased). This preference for the phased side is in agreement with observations in low temperature D_2 [13,15,17], but not with the observation in solid H_2 [12,19]. In these previous studies, the authors offered the explanation that Raman-induced self-focusing at high intensities which favors the phased state is the likely source of their observation [31]. But since our calculation used a top-hat transverse profile and ignored radial variation in the transverse direction, self-focusing could not have been involved in our results. Instead, Le Kien *et al.* [19] pointed out that in efficient adiabatic collinear sideband generation, the molecule must be prepared as a pure or nearly pure antiphased state or phased state with a near-maximum coherence. This can be the case only if the large-coherence condition [Eq. (8)] and the adiabatic-following condition

$$|\Omega_{ab}^{(0)}| \ll T|\delta|^2, \tag{13}$$

where T is the full width at half maximum (FWHM) of the driving laser pulses and $\Omega_{ab}^{(0)}$ denotes that the value of Ω_{ab} at

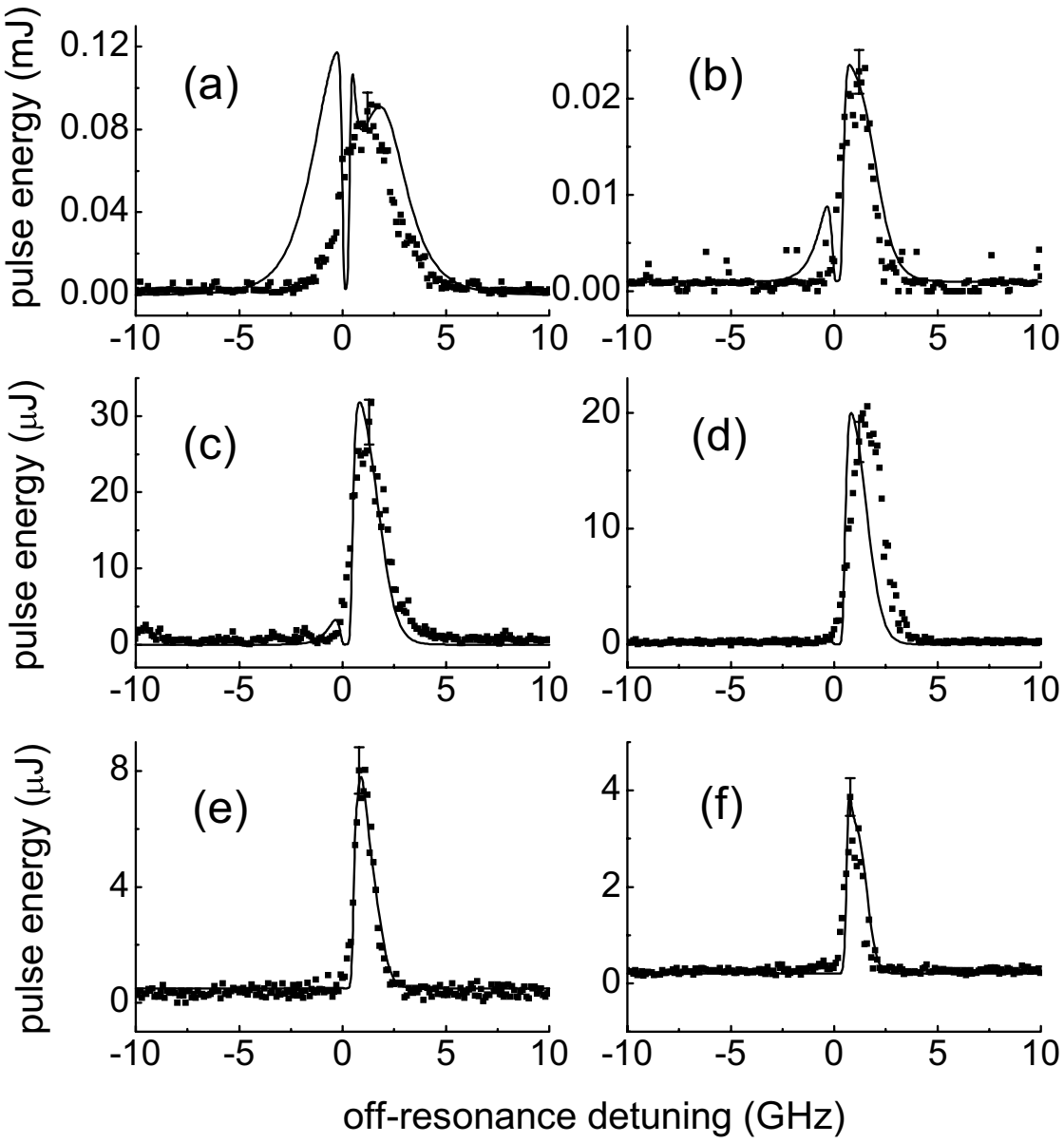

FIG. 9. Measured energies of representative anti-Stokes radiation generated in 500 Torr H_2 for sideband orders: (a) $q=3$, (b) $q=5$, (c) $q=6$, (d) $q=7$, (e) $q=8$, and (f) $q=9$. Square dots are the experimental data points. The solid lines are values calculated under the experimental conditions used and matched to the highest measured output at positive detuning. There are no other free parameters. The error bar indicates the typical one standard deviation fluctuation of the signal near its peak value.

the peak of the pulses are both satisfied. Figure 6 shows the regions of detuning in which both conditions can be satisfied at the intensity level of Fig. 4(c). We see immediately that only for positive detunings with a magnitude of about 1 GHz are both conditions met. For low order ($q \leqslant 3$) sidebands, strict adherence to the large coherence condition is not as important; generation in the antiphased or the phased side could be of the same order of magnitude.

V. COMPARISON WITH EXPERIMENT

The calculations validate the feasibility to achieve efficient molecular modulation in room temperature H_2 at medium high pressure. We now describe our experiments aimed at verifying these simulated results and to generate a broad Raman spectrum suitable for subfemtosecond pulse train construction in room temperature H_2. The experiments employed two pulse-amplified cw single-longitudinal-mode lasers: A dye laser fixed at 589 nm and a Ti:sapphire laser tuned around 780 nm. We set the frequency difference of these two lasers to be approximately equal to 4155 cm^{-1}. The duration of the laser pulses were 5 ns. The pulse energies were 17 and 25 mJ, respectively. The two laser pulses were linearly polarized that were parallel to each other. The pulses were combined and focused to diameters of 190 and 180 μm respectively into the center of a 100 cm long cell containing H_2 at 300 K, yielding an intensity at the focal spot of 20 GW/cm^2 for the 780 nm beam and 12 GW/cm^2

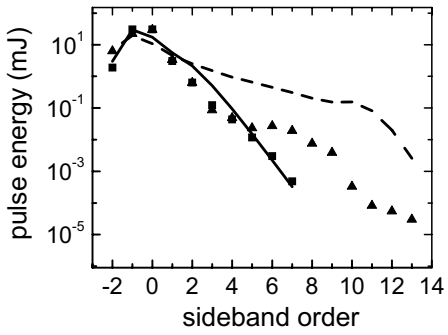

FIG. 10. Comparison of calculated output with measured data for different Stokes and anti-Stokes orders. The solid line is calculated under the experimental conditions in 200 Torr H_2 and the solid squares are the corresponding experimental data points. The dashed line is calculated under the experimental conditions in 500 Torr H_2 and the solid triangles are the corresponding experimental data points.

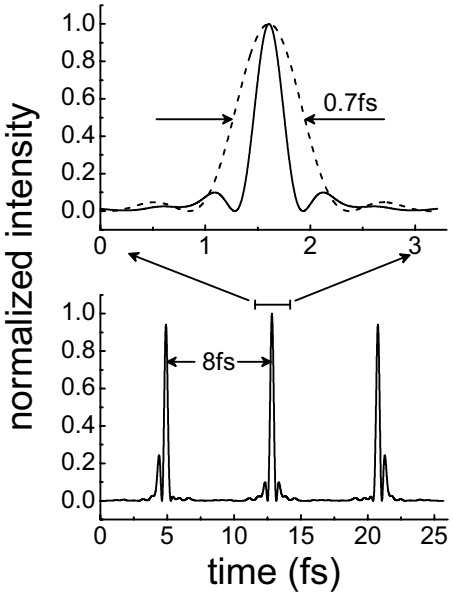

FIG. 11. Bottom figure: Subfemtosecond pulse train estimated from the measured broad spectrum at 500 Torr. The pulse train is obtained by Fourier synthesis of sidebands from the −2nd to 9th order with the assumption that the sideband energies from −2nd to 2nd order are reduced to be the same value as the 3rd order and the phases of all the sidebands are tuned equal. The top figure is an expanded view of the central pulse.

for the 589 nm beam. Under these conditions, the driven Raman coherence could reach 0.44 as its maximum value. The 589 nm pulse was delayed by 1 ns relative to the 780 nm pulse. Hydrogen pressure in the cell was varied from <1 to 1000 Torr. The bandwidths of the lasers were both $\sim$100 MHz.

Coherent output from the cell was dispersed with a suprasil Pellin-Broca prism. The pulse energy of the generated Raman sidebands that has a wavelength longer than 200 nm was measured with a Molectron PS-10 thermopile. Part of the output was reflected off the surface of a MgF_2 plate into a vacuum UV monochromator (McPherson 234/302) for wavelength and relative energy analysis of the output whose wavelengths were shorter than 210 nm (Fig. 7). Two different detectors were used: A solar-blind photomultiplier (Hamamatsu R1459), and a McPherson Model 654 detector assembly that can detect from the vacuum UV to beyond 400 nm. The relative wavelength response of both detectors was determined with a deuterium discharge lamp, and the absolute response was calibrated at 199 nm with an energy meter. Signals from the detectors were integrated with a boxcar signal averager, digitized and recorded by a PC. Each data point was the average of 60 laser pulses.

The two driving lasers generated a collinear beam of Raman sidebands. We scanned the wavelength of the 780 nm beam to vary the magnitude of the coherence. At pressures below 50 Torr, only a few low order Stokes and anti-Stokes radiation were generated and their intensities were low. Above 200 Torr we obtained measurable collinear radiation from the second Stokes to the seventh anti-Stokes order. The number of observed anti-Stokes sidebands increased with H_2 pressure. At 500 Torr, a total of 13 anti-Stokes orders can be recorded. At this pressure, the coherent output contains equally spaced spectral components that range from the infrared to the uv, spanning four octaves to cover over 70 600 cm^{-1} in the optical to deep uv spectral region. The conversion from the pump pulse to the sum of all the sidebands reaches its highest value for an efficiency of 30% at a detuning of 1500 MHz. A full description of the experiment and results will be presented in a forthcoming publication. In this paper, we compare simulated results with the experimental data. The recorded energies at 200 Torr and at 500 Torr as a function of the detuning from the Raman resonance for several sideband orders are shown in Figs. 8 and 9, respectively. The position for zero detuning in these figures was determined by measuring the first anti-Stokes signal spectrum at 100 Torr pressure and reducing the intensity of both laser beams until the position of the signal peak stopped shifting in wavelength. This happened at an intensity of a few hundred MW/cm^2 for both beams. The wavelength where the centroid of the peak signal occurred was then used as the wavelength of the zero detuning position. Simulated results scaled to match the highest energy on the positive detuning side are also displayed in these figures. There is excellent functional agreement between theory and experiment, especially for the higher order sidebands ($q>3$). This agreement lends credibility to the discussion in Sec. IV that the preference to positive detuning in high order sideband generation is mainly a direct consequence of the adiabatic following and large coherence requirements in collinear molecular modulation. Raman induced self-focusing plays only a secondary role in the final observation.

In Fig. 10 we show the pulse energy of the sideband orders from both the simulation and the measurements. Since different sideband orders peak at a slightly different detuning, we plot the maximum achievable pulse energies irrespective of detuning for each order. The experimental observations are in very good agreement with the simulated results at 200 Torr. At 500 Torr, there is a clear discrepancy between predicted and measured pulse energies for the high order sidebands. The cause of this discrepancy is not clear at

this point and requires further investigation. However, we believe this discrepancy in part is a result that the coherence of the laser pulse is less than perfect and is worse than what is used in the calculation so that the effect of collisional dephasing is felt sooner in the experiment than in the simulation. For $q \geqslant 9$ both experiment and calculation show a fast drop in generated pulse energy. The Rayleigh range in the experiment was 3 cm while at 500 Torr the coherence length for the 8th order anti-Stokes generation is 3.2 cm. Thus collinear generation above the 8th order will be affected by phase matching and naturally becomes smaller as destructive interference begins to set in. As we increase to higher pressures the negative influence by these factors on molecular modulation is ever more obvious. At 700 Torr, although the largest number of anti-Stokes orders, 15, was recorded, the output beam at the orders $q > 7$ showed an obvious off-axis component signifying that noncollinear (off-angle phase-matching) generation has begun to dominate.

Finally we estimate the subfemtosecond pulse train that one can get using the measured broad spectrum at 500 Torr. Figure 11 is obtained by Fourier synthesis of sidebands from the −2nd to 9th order with the assumption that the sideband energies from −2nd to 2nd order are reduced to the same value as the 3rd order and the phases of all the sidebands are tuned equal. The figure shows a single cycle electric field with a width of ~0.3 fs while the FWHM of the intensity envelope shown is ~0.7 fs. The pulse separation is 8 fs and the peak pulse power is nearly 1 MW.

VI. CONCLUSION

In summary, we have presented the details of our numerical calculation including comparison with the results of experiments for vibrational molecular modulation in room temperature H_2. We showed that while collisions are damaging in most coherent processes, they play an important role in realizing efficient modulation in room temperature H_2 where Dicke narrowing reduces the Doppler width to minimize the destructive contributions from opposite wings in the Doppler profile to the molecular coherence. In addition, generation of high order sidebands favors the phased state and is primarily a consequence of the resulting Stark shifts due to the high intensities applied. The influence of self-focusing in the gas is only secondary. Experimentally we succeeded in generating collinearly propagating sidebands with wavelengths that range from 2216 nm in the infrared to 133 nm in the vacuum UV. The frequency range covered by these sidebands spans over four octaves for a total width of more than 70 600 cm^{-1} in the optical region of the spectrum. Such a spectrum could be used in the reconstruction of single-cycle waveforms in the visible and/or uv region. Our simulation shows that a pulse train with a single-cycle pulse width of 0.3 fs, a pulse separation of 8 fs, and a peak power of nearly 1 MW is achievable. Molecular modulated H_2 can also be an excellent medium for producing intense tunable deep uv radiation by adding a third tunable laser to the system [32] or as a source of THz repetition rate electromagnetic radiation [33].

ACKNOWLEDGMENTS

We thank K. Hakuta and Fam Le Kien for helpful discussions and Fam Le Kien for providing us his matrix elements data used in the current calculations. This work was supported by the Academia Sinica and the National Science Council.

[1] G. Farkas and C. Toth, Phys. Lett. A **168**, 447 (1992).
[2] S. E. Harris, J. J. Macklin, and T. W. Hansch, Opt. Commun. **100**, 487 (1993).
[3] P. B. Corkum, N. H. Burnett, and M. Y. Ivanov, Opt. Lett. **19**, 1870 (1994).
[4] P. Antoine, A. L'Huillier, and M. Lewenstein, Phys. Rev. Lett. **77**, 1234 (1996).
[5] K. J. Schafer and K. C. Kulander, Phys. Rev. Lett. **78**, 638 (1997).
[6] R. Lopez-Martens, K. Varju, P. Johnsson, J. Mauritsson, Y. Mairesse, P. Salieres, M. B. Gaarde, K. J. Schafer, A. Persson, S. Svanberg, C. G. Wahlstrom, and A. L'Huillier, Phys. Rev. Lett. **94**, 033001 (2005).
[7] K. Hakuta, M. Suzuki, M. Katsuragawa, and J. Z. Li, Phys. Rev. Lett. **79**, 209 (1997).
[8] S. E. Harris and A. V. Sokolov, Phys. Rev. A **55**, R4019 (1997).
[9] S. E. Harris and A. V. Sokolov, Phys. Rev. Lett. **81**, 2894 (1998).
[10] A. V. Sokolov, Opt. Lett. **24**, 1248 (1999).
[11] A. V. Sokolov, D. D. Yavuz, and S. E. Harris, Opt. Lett. **24**, 557 (1999).
[12] J. Q. Liang, M. Katsuragawa, F. Le Kien, and K. Hakuta, Phys. Rev. Lett. **85**, 2474 (2000).
[13] A. V. Sokolov, D. R. Walker, D. D. Yavuz, G. Y. Yin, and S. E. Harris, Phys. Rev. Lett. **85**, 562 (2000).
[14] A. V. Sokolov, D. D. Yavuz, D. R. Walker, G. Y. Yin, and S. E. Harris, Phys. Rev. A **63**, 051801 (2001).
[15] D. D. Yavuz, D. R. Walker, G. Y. Yin, and S. E. Harris, Opt. Lett. **27**, 769 (2002).
[16] D. D. Yavuz, D. R. Walker, M. Y. Shverdin, G. Y. Yin, and S. E. Harris, Phys. Rev. Lett. **91**, 233602 (2003).
[17] S. Gundry, M. P. Anscombe, A. M. Abdulla, S. D. Hogan, E. Sali, J. W. G. Tisch, and J. P. Marangos, Phys. Rev. A **72**, 033824 (2005).
[18] M. Y. Shverdin, D. R. Walker, D. D. Yavuz, G. Y. Yin, and S. E. Harris, Phys. Rev. Lett. **94**, 033904 (2005).
[19] F. Le Kien, J. Q. Liang, M. Katsuragawa, K. Ohtsuki, K. Hakuta, and A. V. Sokolov, Phys. Rev. A **60**, 1562 (1999).
[20] G. Herzberg, *Molecular Spectra and Molecular Structure. I. Spectra of Diatomic Molecules* (Van Nostrand Reinhold, New York, 1950).
[21] A. C. Allison and A. Dalgarno, At. Data **1**, 289 (1970).
[22] A. Owyoung, Opt. Lett. **2**, 91 (1978).
[23] J. D. Kelley and S. L. Bragg, Phys. Rev. A **34**, 3003 (1986).
[24] R. Lucht and R. Farrow, J. Opt. Soc. Am. B **5**, 1243 (1988).

[25] R. Dicke, Phys. Rev. **89**, 472 (1953).
[26] R. Romer and R. Dicke, Phys. Rev. **99**, 532 (1955).
[27] F. Le Kien (private communication).
[28] A. Dalgarno and D. A. Williams, Proc. Phys. Soc. London **85**, 685 (1965).
[29] S. Gill, Proc. Cambridge Philos. Soc. **47**, 96 (1951).
[30] E. Solodovnik, G. Cokkinides, and A. Sakis Meliopouls, Proceedings of the Thirtieth Southeastern Symposium on System Theory (unpublished).
[31] D. R. Walker, D. D. Yavuz, M. Y. Shverdin, G. Y Yin, A. V. Sokolov, and S. E. Harris, Opt. Lett. **27**, 2094 (2002).
[32] W.-J. Chen and A.H. Kung, Opt. Lett. **30**, 2608 (2005).
[33] M. Katsuragawa, K. Yokoyama, T. Onose, and K. Misawa, Opt. Express **13**, 5628 (2005).